

Supporting Information

A Highly-Reversible Room-Temperature Sodium Metal Anode

Zhi Wei Seh, Jie Sun, Yongming Sun, Yi Cui*

*Correspondence should be addressed to: yicui@stanford.edu

Materials and Methods

Materials. All the electrolyte preparation and cell assembly procedures were carried out in an Ar-filled glove box with H₂O and O₂ levels < 0.5 ppm. The electrolyte salts used were sodium hexafluorophosphate (NaPF₆; 99+%, Alfa Aesar), sodium bis(trifluoromethanesulfonyl)imide (NaN(SO₂CF₃)₂ or NaTFSI; 99.5%, Solvionic), sodium bis(fluorosulfonyl)imide (NaN(SO₂F)₂ or NaFSI; 99.7%, Solvionic), sodium trifluoromethanesulfonate (NaSO₃CF₃ or NaOTf; 98%, Alfa Aesar) and sodium perchlorate (NaClO₄; ≥ 98.0%, Sigma-Aldrich). All electrolyte salts were dried thoroughly by heating at 100°C for 24 h in an Ar-filled glove box prior to use. The electrolyte solvents used were diethylene glycol dimethyl ether (diglyme; 99.5%, Sigma-Aldrich), ethylene glycol dimethyl ether (monoglyme; 99.5%, Sigma-Aldrich), tetraethylene glycol dimethyl ether (tetraglyme; > 99%, Solvionic), ethylene carbonate (EC; 99%, Sigma-Aldrich), diethyl carbonate (DEC; ≥ 99%, Sigma-Aldrich) and dimethyl carbonate (DMC; ≥ 99%, Sigma-Aldrich). All electrolyte solvents were anhydrous and used as received. The Na metal used was freshly cut from Na cubes (99.95%, Alfa Aesar).

Electrochemical measurements. 2032-type coin cells were assembled in an Ar-filled glove box using Cu foil working electrode, Na metal counter electrode, Celgard 2325 separator and 25 μ L of electrolyte. Using an 8-channel MTI battery tester, the cells were first cycled at 50 μ A cm⁻² from 0 to 1 V vs. Na⁺/Na for 10 cycles to remove any surface contamination. Galvanostatic plating of Na was then carried out at the desired current density and areal capacity, followed by stripping of Na by charging to a cutoff voltage of 1 V vs. Na⁺/Na, all performed at room temperature. The Coulombic efficiency for each cycle was calculated as the ratio of the capacity of Na stripped to that of Na deposited. The average voltage hysteresis was calculated by dividing the energy by the capacity for both the plating and stripping half-cycle and summing them up. Impedance spectroscopy was carried out in the deposited state after cycling at 0.5 mA cm⁻² and 1 mAh cm⁻², with Cu foil as the working electrode and Na metal as the counter and reference electrodes (Bio-Logic VMP3 Potentiostat; 1 MHz to 1 mHz). Ionic conductivity of the electrolytes was measured at room temperature (20°C) with 2 stainless steel plates using impedance spectroscopy (Bio-Logic VMP3 Potentiostat; 1 MHz to 1 mHz).

Characterization. For characterization using SEM, the Na|Cu cells were disassembled in the deposited state to examine the Na deposited on the Cu foil. For characterization using XPS, the Na|Cu cells were disassembled in the stripped state after 10 plating–stripping cycles at 0.5 mA cm⁻² and 1 mAh cm⁻² to examine the SEI layer remaining on the Cu foil. In both cases, the Cu working electrodes were washed thoroughly using the respective electrolyte solvent (without the salt) prior to analysis. SEM was performed using a FEI Quanta 250 FEG at an accelerating voltage of 5 kV. XPS was carried out using a PHI 5000 VersaProbe with a monochromatic Al K α X-ray source (1,486.7 eV) at 50 W and 16 kV with a beam spot size of 200 μ m. The samples were transferred into the chamber without exposure to air using a sealed Ar-filled vessel. Depth profiling was done

using Ar ion sputtering at 0.5 kV and 0.5 μ A over a 2 x 2 mm area. The thickness of the SEI was estimated from the calibrated sputtering rate of 1 nm per min in SiO₂ and the sputtering time at which the atomic concentration of Na drops to < 5% (by measurement or extrapolation). The Cu 2p3/2 peaks arise due to the underlying Cu foil.

Na–S battery. First, to synthesize the sulfur/carbon (S/C) cathode, C nanofibers were prepared using a modified oxidative template assembly method. Cetyltrimethylammonium bromide (7.3 g) was dissolved in a 1 M HCl solution (120 mL) in an ice bath, followed by addition of ammonium persulfate (13.7 g) and pyrrole monomer (8.3 mL). After reaction for 24 h, the as-synthesized polypyrrole nanofibers were washed with 1 M HCl and deionized water, followed by annealing at 700°C for 3 h under N₂ atmosphere to obtain C nanofibers. The C nanofibers were then mixed with commercial S in a weight ratio of 1: 1 and heated in a sealed stainless steel autoclave at 155°C for 24 h and 350°C for 6 h for infiltration of S. The as-synthesized S/C composites were mixed with conductive Super P and polyvinylidene fluoride binder in a weight ratio of 8: 1: 1 and dispersed in *N*-methyl-2-pyrrolidinone to form a slurry, which was then coated onto Al foil using doctor blade and dried at 60°C under vacuum to form the cathode. 2032-type coin cells were assembled in an Ar-filled glove box using the S/C cathode, Na metal anode, glass microfiber separator (GF/D) and 25 μ L of electrolyte. An additional 0.2 M of NaNO₃ was added to 1 M NaPF₆ and NaN(SO₂CF₃)₂ in tetraglyme to reduce the polysulfide shuttle effect (NaNO₃ cannot be dissolved in 1 M NaPF₆ in 1: 1 v/v EC/DEC). Galvanostatic cycling was carried out at 0.1C (1C = 1,673 mA g⁻¹) from 1.2 to 2.8 V vs. Na⁺/Na at room temperature and specific capacities were calculated based on the mass of S.

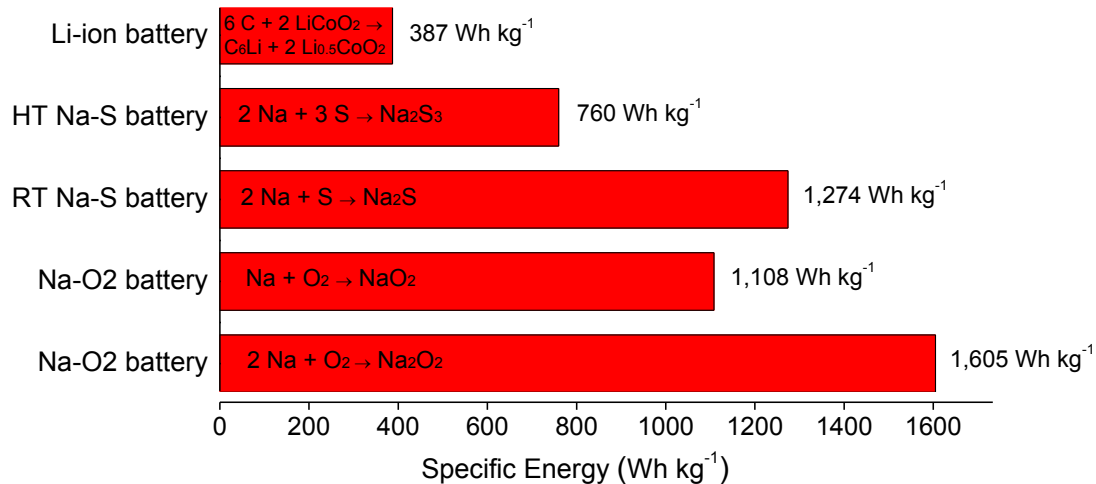


Fig. S1 Specific energy values of various Na-metal batteries in comparison with conventional Li-ion batteries based on graphite anodes and LiCoO₂ cathodes.¹⁻⁴ HT Na–S battery refers to existing high-temperature Na–S batteries operating at 300 to 350°C which use molten Na anode and S cathode with beta-alumina solid electrolyte.² It allows only partial discharge to molten Na₂S₃ because further discharge will cause solid Na₂S₂ and Na₂S to precipitate out. RT Na–S battery refers to room-temperature Na–S batteries which use solid Na anode and S cathode with liquid electrolyte, allowing complete discharge to Na₂S.³ For Na–O₂ batteries, there are 2 possible discharge products, NaO₂ and Na₂O₂, depending on the specific conditions used. In particular, the formation of NaO₂ as the discharge product was found to result in low charge–discharge overpotential during cycling.⁴

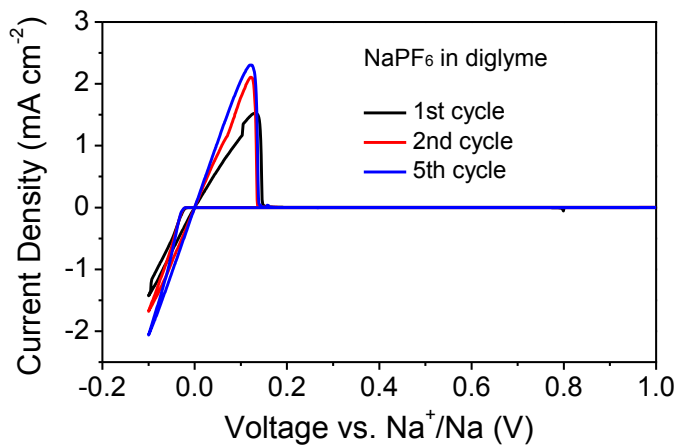


Fig. S2 Cyclic voltammograms of Na plating and stripping using 1 M NaPF_6 in diglyme, carried out using a Bio-Logic VMP3 Potentiostat (scan rate: 0.1 mV s^{-1}) with Cu foil as the working electrode and Na metal as the counter and reference electrodes.

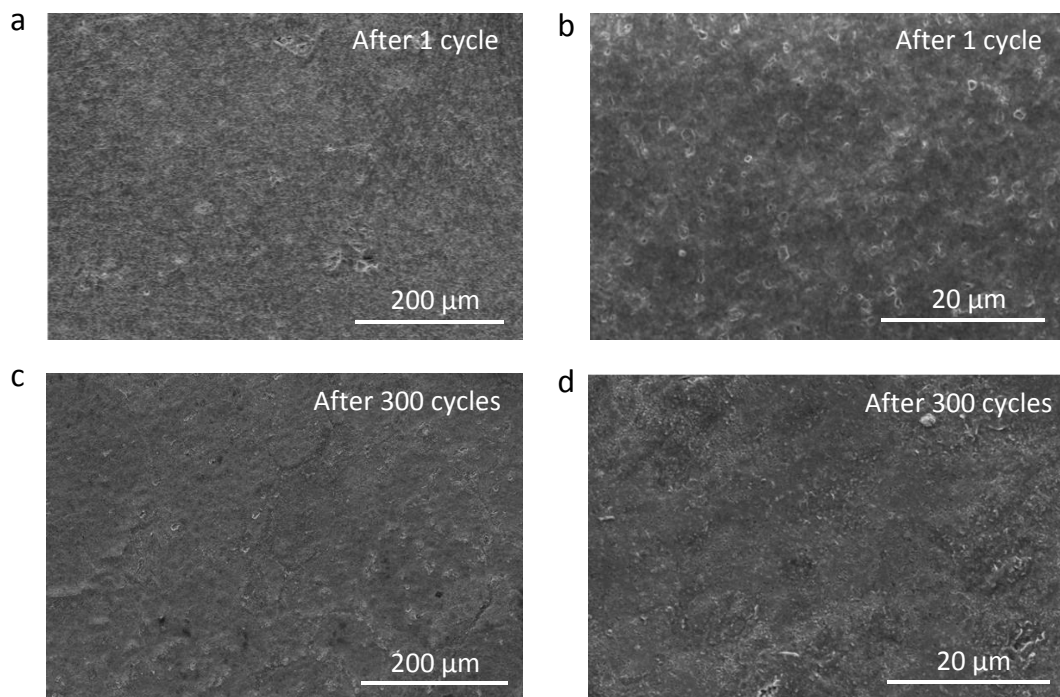


Fig. S3 Low- and high-magnification SEM images of the Na metal surface (**a, b**) after 1 cycle and (**c, d**) after 300 cycles at 0.5 mA cm^{-2} and 1 mAh cm^{-2} using 1 M NaPF_6 in diglyme.

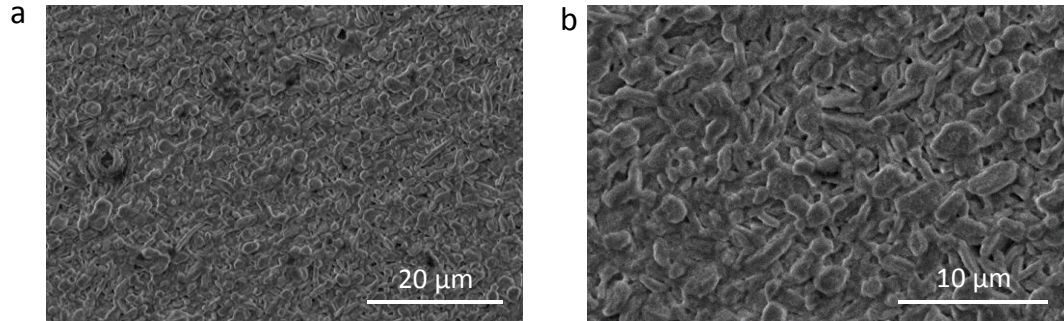


Fig. S4 (a) Low- and (b) high-magnification SEM images of the Na metal surface showing regions of nodule-like Na deposits, cycled at 0.5 mA cm^{-2} and 1 mAh cm^{-2} using 1 M NaPF_6 in diglyme.

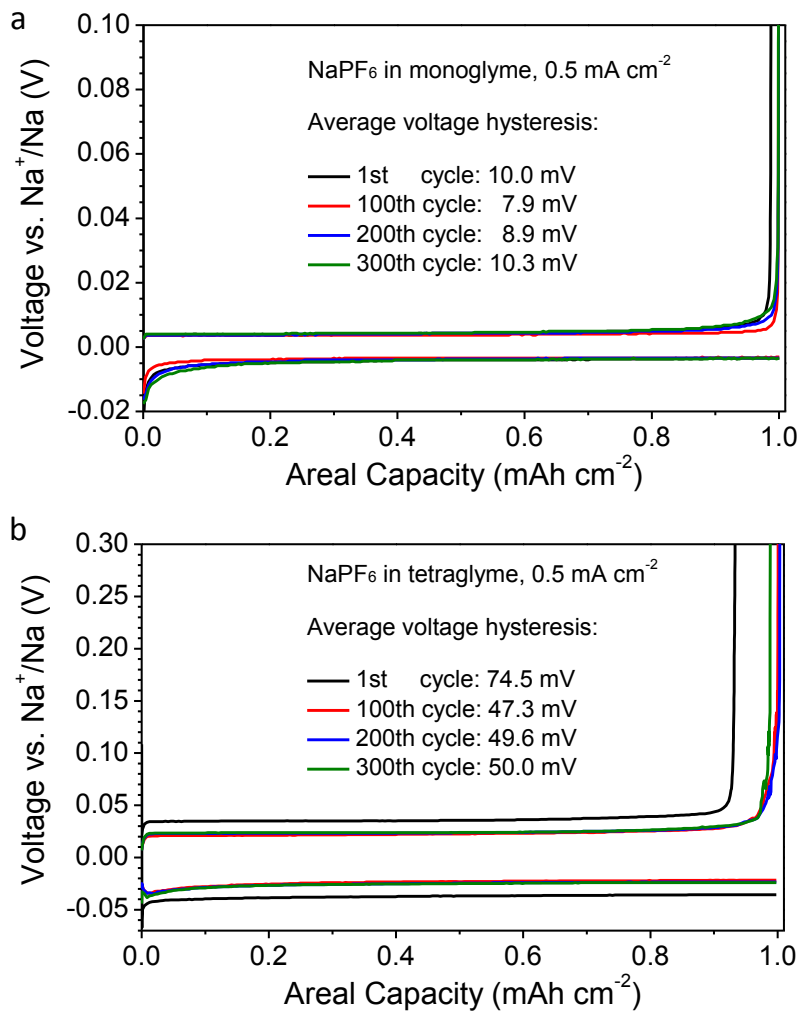


Fig. S5 Plating–stripping voltage profiles and average voltage hysteresis of Na metal anodes cycled at 0.5 mA cm^{-2} and 1 mAh cm^{-2} using (a) 1 M NaPF_6 in monoglyme and (b) 1 M NaPF_6 in tetraglyme.

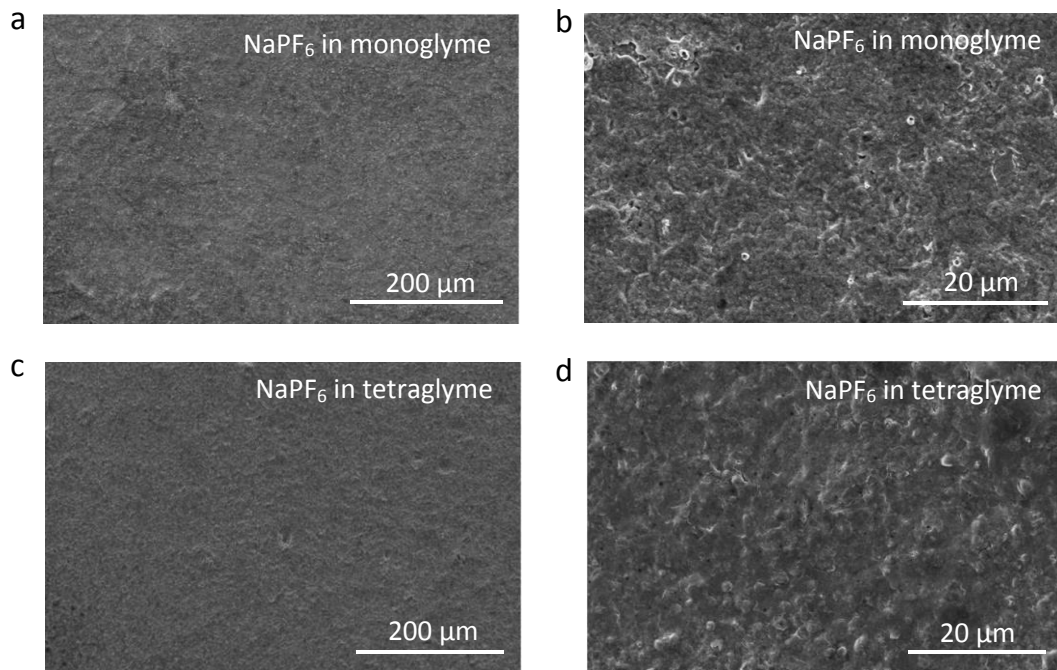


Fig. S6 Low- and high-magnification SEM images of the Na metal surface after 1 cycle at 0.5 mA cm^{-2} and 1 mAh cm^{-2} using (a, b) 1 M NaPF_6 in monoglyme and (c, d) 1 M NaPF_6 in tetraglyme.

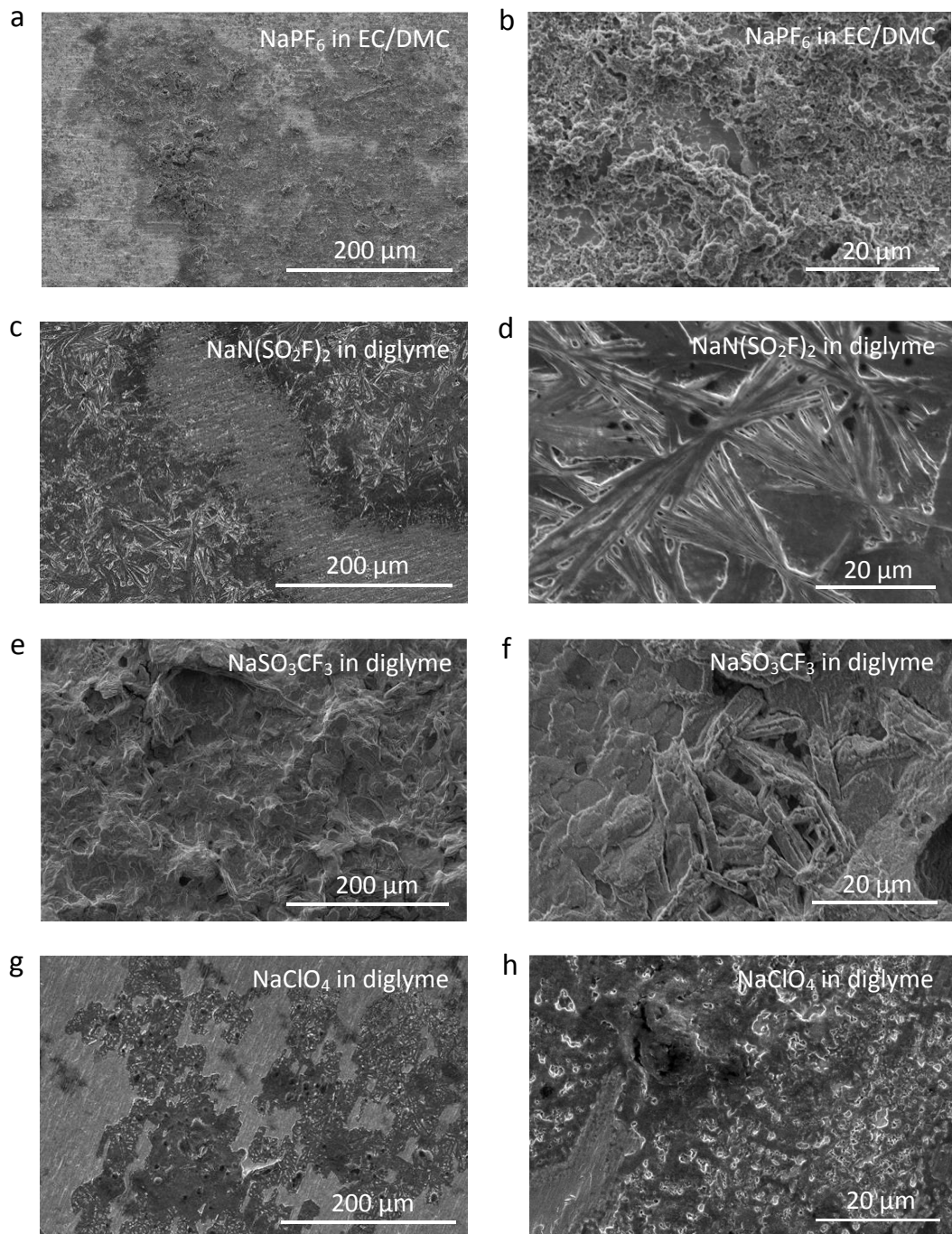


Fig. S7 Low- and high-magnification SEM images of the Na metal surface after 1 cycle at 0.5 mA cm^{-2} and 1 mAh cm^{-2} using (a, b) 1 M NaPF_6 in 1: 1 v/v EC/DMC, (c, d) 1 M $\text{NaN}(\text{SO}_2\text{F})_2$ in diglyme, (e, f) 1 M NaSO_3CF_3 in diglyme and (g, h) 1 M NaClO_4 in diglyme.

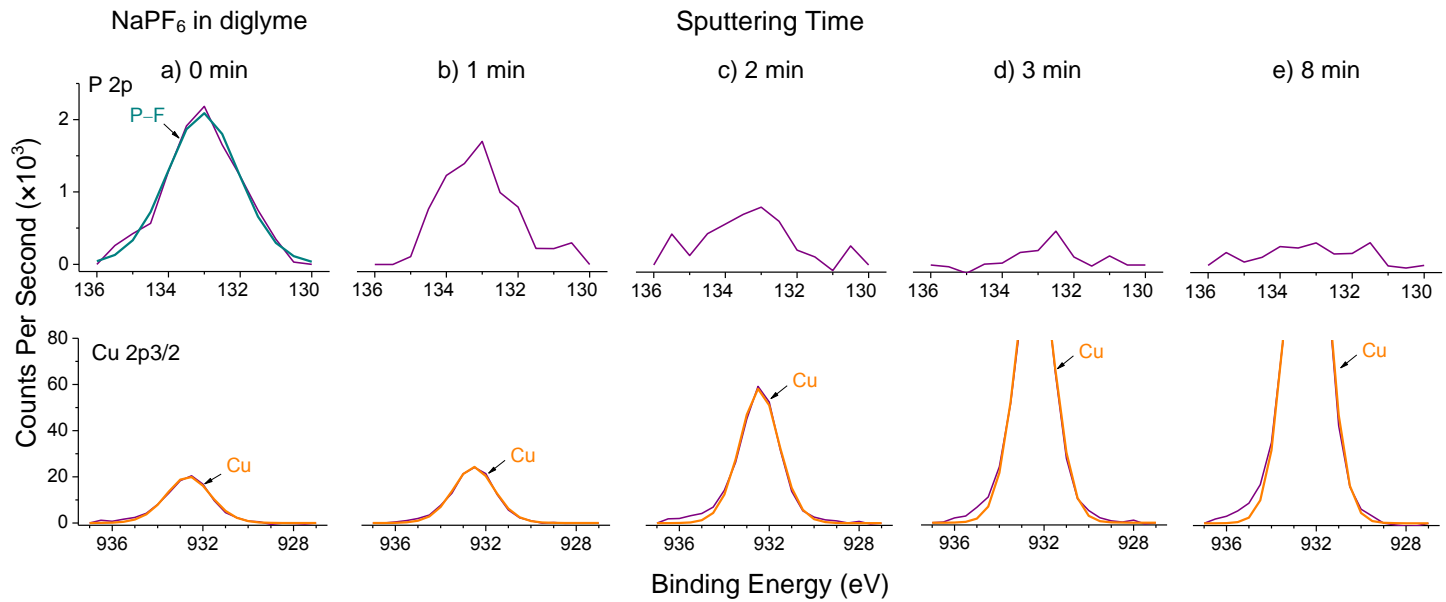


Fig. S8 XPS characterization of the SEI formed using 1 M NaPF_6 in diglyme after (a) 0 min, (b) 1 min, (c) 2 min, (d) 3 min and (e) 8 min of sputtering, supplementary to Fig. 4. The Cu 2p_{3/2} peaks arise due to the underlying Cu foil.

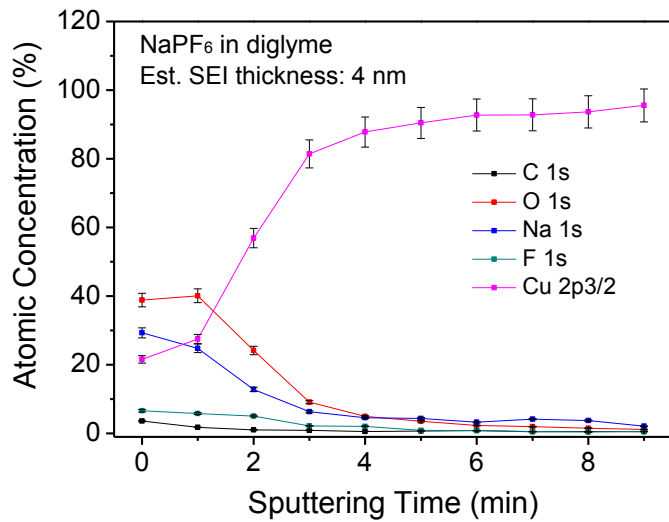


Fig. S9 XPS atomic concentration of various elements as a function of sputtering time for the SEI formed using 1 M NaPF_6 in diglyme. The thickness of the SEI was estimated from the calibrated sputtering rate of 1 nm per min in SiO_2 and the sputtering time at which the atomic concentration of Na drops to < 5%. The Cu 2p_{3/2} peaks arise due to the underlying Cu foil.

Table S1 XPS binding energy values and peak assignments of the SEI components formed using 1 M NaPF₆ in diglyme.⁵⁻¹⁰ The Cu 2p3/2 peaks arise due to the underlying Cu foil.

NaPF ₆ in diglyme		Binding energy (eV)					
Sputtering time	0 min	1 min	2 min	3 min	8 min	Peak assignment	Species
C 1s	288.2	-	-	-	-	C–O	RCH ₂ ONa
	284.8	-	-	-	-	C–C, C–H	RCH ₂ ONa
O 1s	535.5	-	-	-	-	C–O	RCH ₂ ONa
	530.9	530.7	530.3	-	-	Na–O	Na ₂ O
Na 1s	1071.0	1071.3	1071.1	-	-	Na–O, Na–F	Na ₂ O, NaF
	686.4	-	-	-	-	P–F	Na _x PF _y , Na _x PO _y F _z
F 1s	683.8	684.3	684.6	-	-	Na–F	NaF
	133.0	-	-	-	-	P–F	Na _x PF _y , Na _x PO _y F _z
Cu 2p3/2	932.6	932.5	932.4	932.4	932.4	Cu	Cu

Table S2 Mechanical properties of Na metal and various SEI components in this work.¹¹⁻¹⁵

	Na	Na ₂ O	NaF	NaCl
Shear modulus (GPa)	3.3	49.7	31.4	15.8
Young's modulus (GPa)	10.0	116.1	77.4	39.2
Bulk modulus (GPa)	6.3	58.3	48.3	25.3

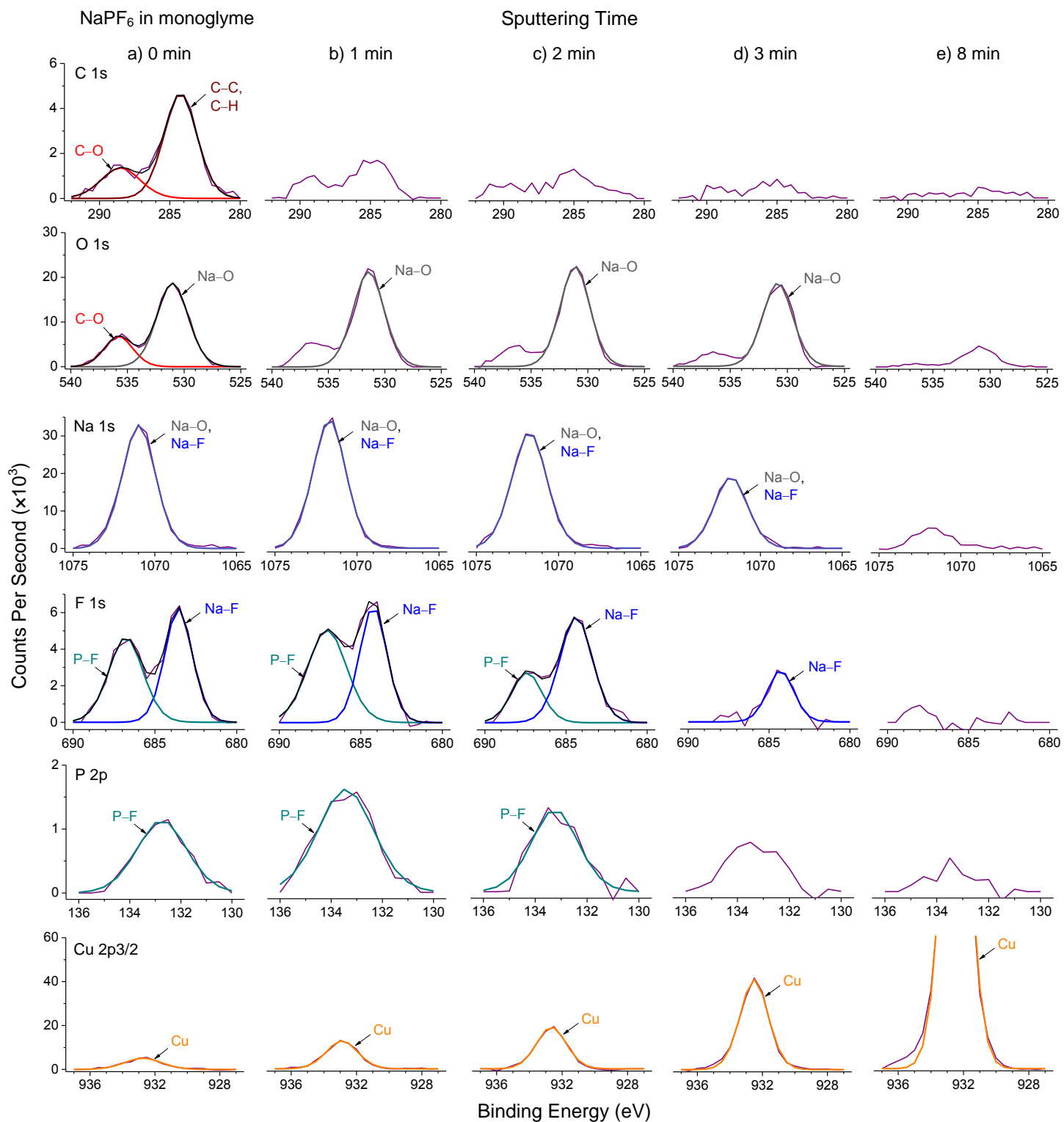


Fig. S10 XPS characterization of the SEI formed using 1 M NaPF₆ in monoglyme after (a) 0 min, (b) 1 min, (c) 2 min, (d) 3 min and (e) 8 min of sputtering.

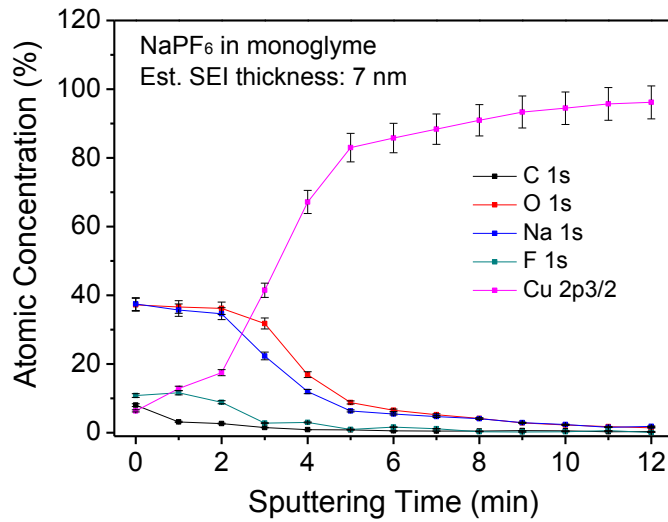


Fig. S11 XPS atomic concentration of various elements as a function of sputtering time for the SEI formed using 1 M NaPF₆ in monoglyme.

Table S3 XPS binding energy values and peak assignments of the SEI components formed using 1 M NaPF₆ in monoglyme.⁵⁻¹⁰

NaPF ₆ in monoglyme		Binding Energy (eV)					
Sputtering time	0 min	1 min	2 min	3 min	8 min	Peak assignment	Species
C 1s	288.5	-	-	-	-	C–O	RCH ₂ ONa
	284.2	-	-	-	-	C–C, C–H	RCH ₂ ONa
O 1s	535.5	-	-	-	-	C–O	RCH ₂ ONa
	531.0	531.4	531.1	530.8	-	Na–O	Na ₂ O
Na 1s	1071.0	1071.7	1071.8	1071.8	-	Na–O, Na–F	Na ₂ O, NaF
	686.8	687.1	687.4	-	-	P–F	Na _x PF _y , Na _x PO _y F _z
F 1s	683.5	684.2	684.4	684.3	-	Na–F	NaF
	132.7	133.4	133.2	-	-	P–F	Na _x PF _y , Na _x PO _y F _z
Cu 2p3/2	932.7	932.9	932.6	932.5	932.5	Cu	Cu

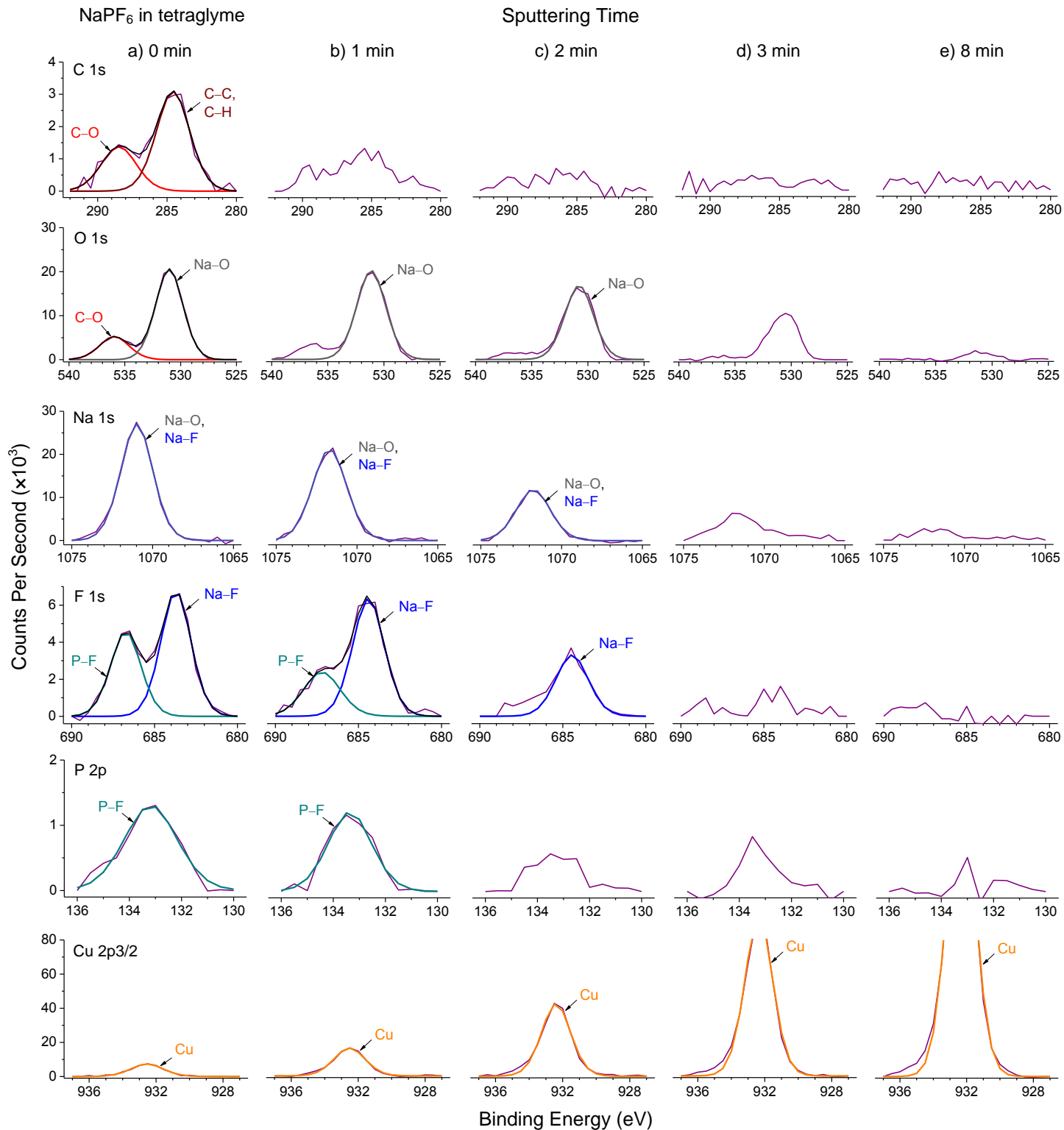


Fig. S12 XPS characterization of the SEI formed using 1 M NaPF₆ in tetraglyme after **(a)** 0 min, **(b)** 1 min, **(c)** 2 min, **(d)** 3 min and **(e)** 8 min of sputtering.

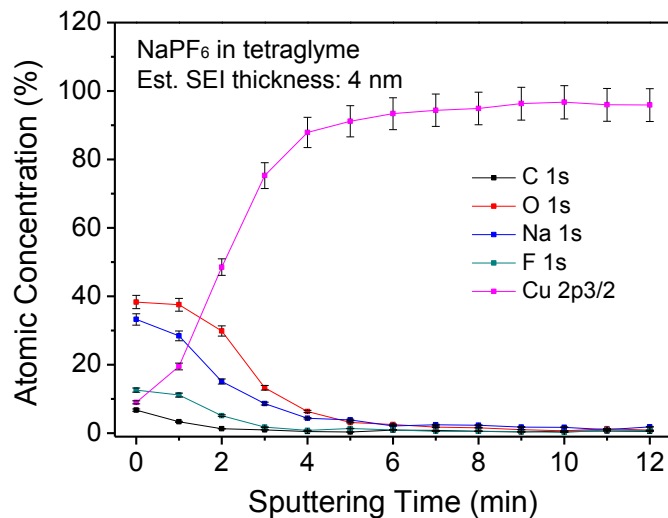


Fig. S13 XPS atomic concentration of various elements as a function of sputtering time for the SEI formed using 1 M NaPF₆ in tetraglyme.

Table S4 XPS binding energy values and peak assignments of the SEI components formed using 1 M NaPF₆ in tetraglyme.⁵⁻¹⁰

NaPF ₆ in tetraglyme		Binding Energy (eV)					
Sputtering time	0 min	1 min	2 min	3 min	8 min	Peak assignment	Species
C 1s	288.5	-	-	-	-	C–O	RCH ₂ ONa
	284.6	-	-	-	-	C–C, C–H	RCH ₂ ONa
O 1s	535.9	-	-	-	-	C–O	RCH ₂ ONa
	531.0	531.1	530.8	-	-	Na–O	Na ₂ O
Na 1s	1071.0	1071.7	1071.7	-	-	Na–O, Na–F	Na ₂ O, NaF
F 1s	686.7	687.2	-	-	-	P–F	Na _x PF _y , Na _x PO _y F _z
	683.7	684.4	684.4	-	-	Na–F	NaF
P 2p	133.2	133.4	-	-	-	P–F	Na _x PF _y , Na _x PO _y F _z
Cu 2p3/2	932.5	932.5	932.4	932.3	932.3	Cu	Cu

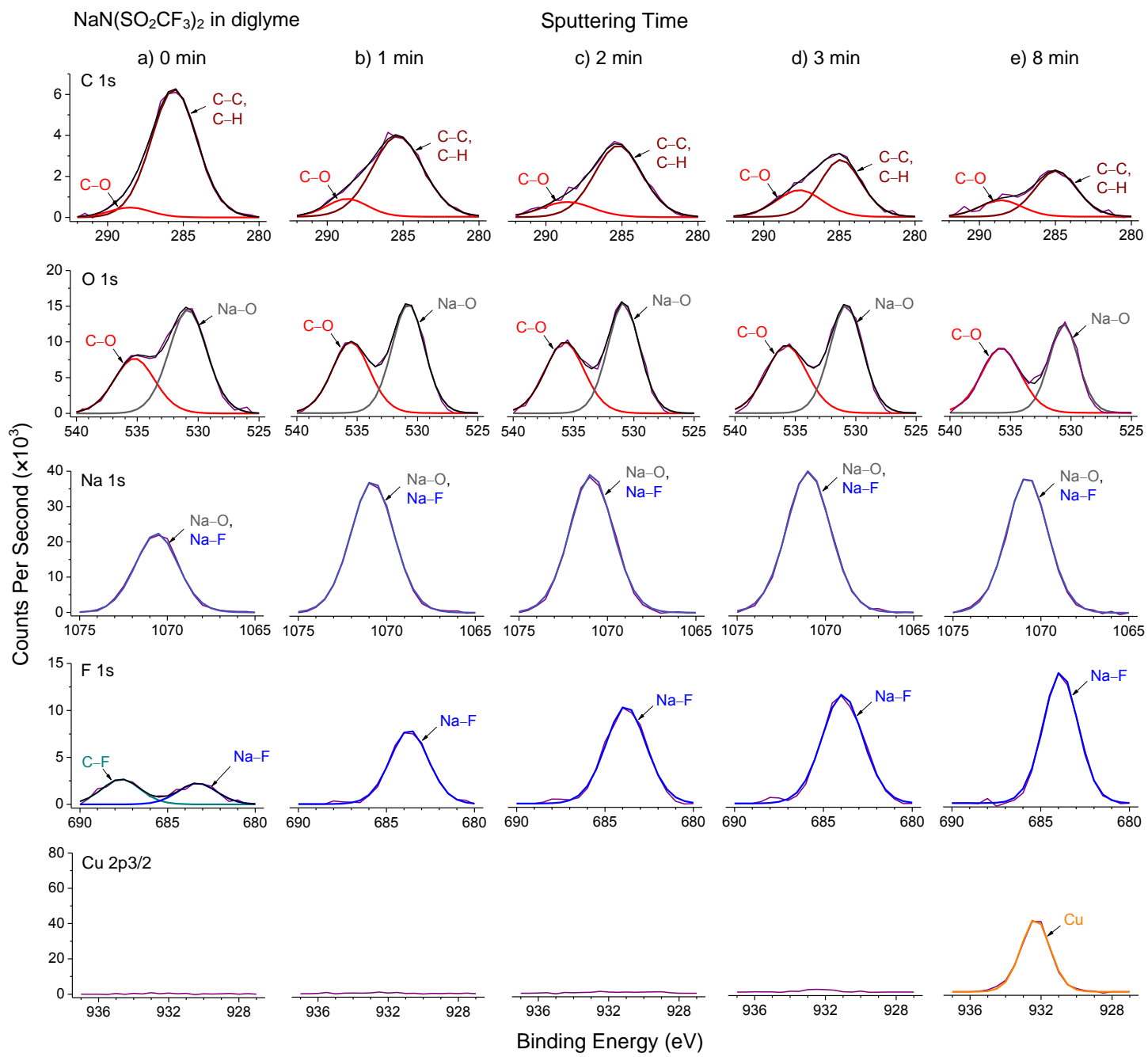


Fig. S14 XPS characterization of the SEI formed using 1 M NaN(SO₂CF₃)₂ in diglyme after **(a)** 0 min, **(b)** 1 min, **(c)** 2 min, **(d)** 3 min and **(e)** 8 min of sputtering.

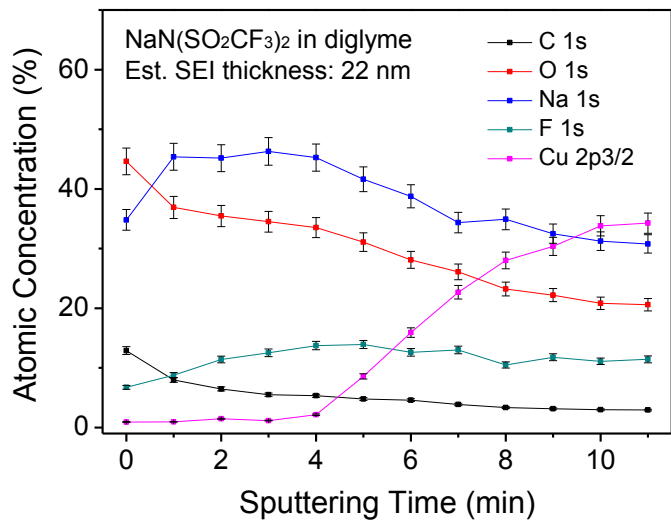


Fig. S15 XPS atomic concentration of various elements as a function of sputtering time for the SEI formed using $1\text{ M } \text{NaN}(\text{SO}_2\text{CF}_3)_2$ in diglyme.

Table S5 XPS binding energy values and peak assignments of the SEI components formed using $1\text{ M } \text{NaN}(\text{SO}_2\text{CF}_3)_2$ in diglyme.⁵⁻¹⁰

$\text{NaN}(\text{SO}_2\text{CF}_3)_2$ in diglyme		Binding Energy (eV)					
Sputtering time	0 min	1 min	2 min	3 min	8 min	Peak assignment	Species
C 1s	288.5	288.7	288.6	287.6	288.6	C–O	RCH_2ONa
	285.6	285.3	285.2	284.9	285.0	C–C, C–H	RCH_2ONa
O 1s	535.2	535.5	535.7	535.7	535.8	C–O	RCH_2ONa
	530.8	530.8	530.8	530.8	530.6	Na–O	Na_2O
Na 1s	1070.6	1070.8	1070.9	1071.0	1070.8	Na–O, Na–F	$\text{Na}_2\text{O}, \text{NaF}$
F 1s	687.7	-	-	-	-	C–F	CF_3
	683.3	683.7	683.8	683.9	683.9	Na–F	NaF
Cu 2p $\frac{3}{2}$	-	-	-	-	932.3	Cu	Cu

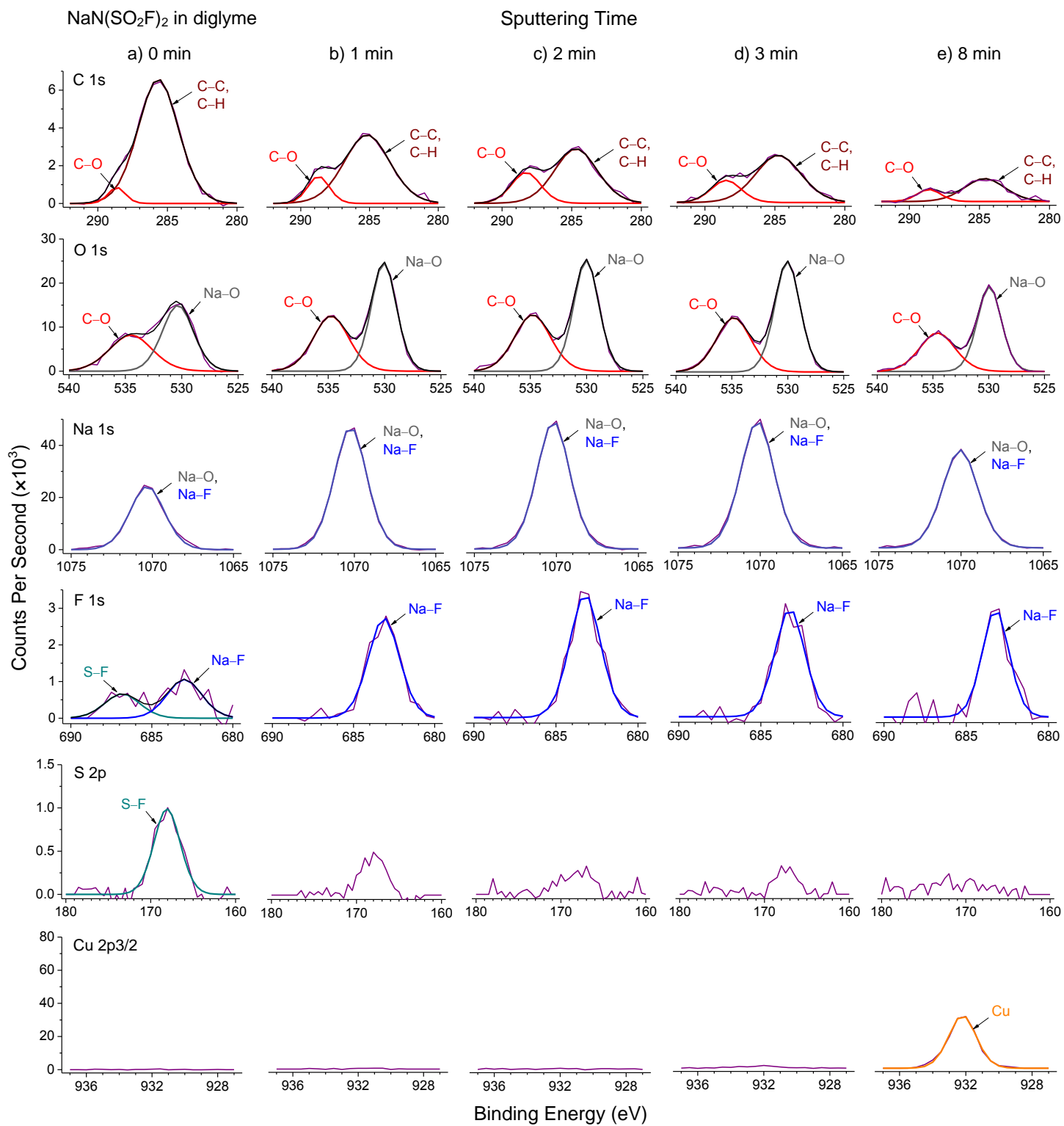


Fig. S16 XPS characterization of the SEI formed using 1 M NaN(SO₂F)₂ in diglyme after **(a)** 0 min, **(b)** 1 min, **(c)** 2 min, **(d)** 3 min and **(e)** 8 min of sputtering.

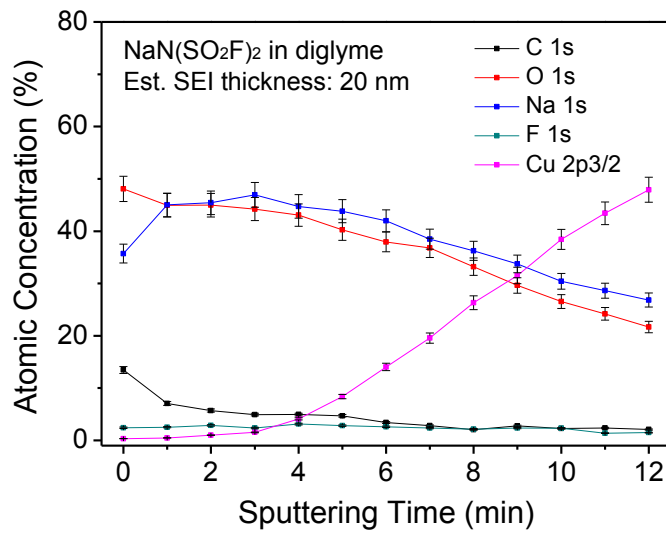


Fig. S17 XPS atomic concentration of various elements as a function of sputtering time for the SEI formed using 1 M NaN(SO₂F)₂ in diglyme.

Table S6 XPS binding energy values and peak assignments of the SEI components formed using 1 M NaN(SO₂F)₂ in diglyme.⁵⁻¹⁰

NaN(SO ₂ F) ₂ in diglyme		Binding Energy (eV)					
Sputtering time	0 min	1 min	2 min	3 min	8 min	Peak assignment	Species
C 1s	288.6	288.7	288.3	288.5	288.6	C–O	RCH ₂ ONa
	285.7	285.2	284.7	284.8	284.6	C–C, C–H	RCH ₂ ONa
O 1s	534.5	534.7	534.8	534.8	534.6	C–O	RCH ₂ ONa
	530.3	530.1	530.0	530.0	529.9	Na–O	Na ₂ O
Na 1s	1070.3	1070.2	1070.2	1070.2	1070.0	Na–O, Na–F	Na ₂ O, NaF
	686.8	-	-	-	-	S–F	SO ₂ F
F 1s	683.0	683.1	683.2	683.2	683.2	Na–F	NaF
	168.1	-	-	-	-	S–F	SO ₂ F
Cu 2p3/2	-	-	-	-	932.2	Cu	Cu

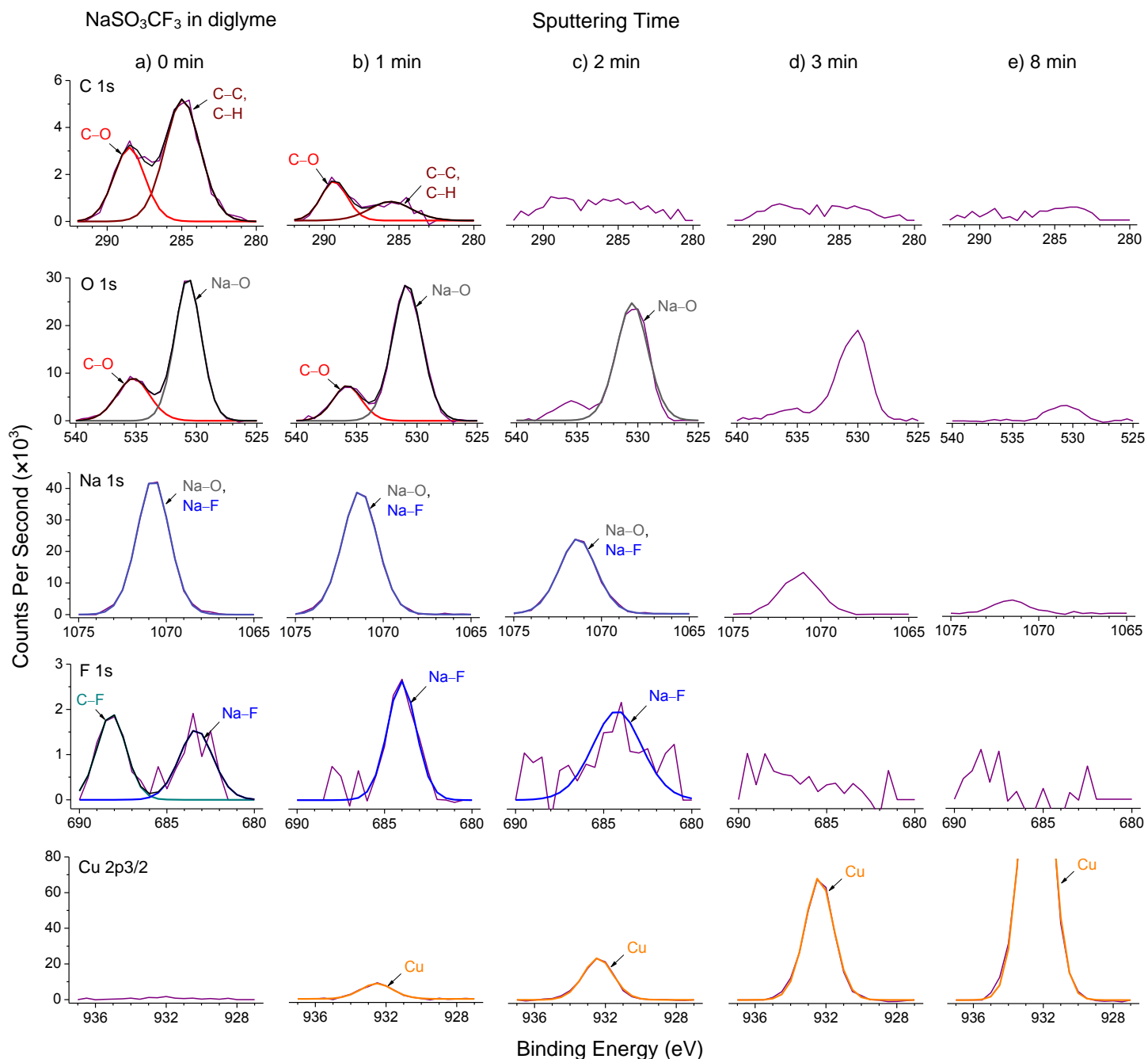


Fig. S18 XPS characterization of the SEI formed using 1 M NaSO₃CF₃ in diglyme after **(a)** 0 min, **(b)** 1 min, **(c)** 2 min, **(d)** 3 min and **(e)** 8 min of sputtering.

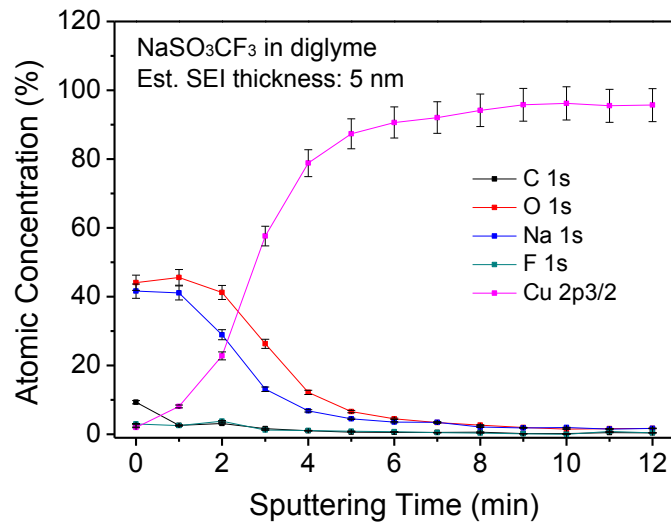


Fig. S19 XPS atomic concentration of various elements as a function of sputtering time for the SEI formed using 1 M NaSO_3CF_3 in diglyme.

Table S7 XPS binding energy values and peak assignments of the SEI components formed using 1 M NaSO_3CF_3 in diglyme.⁵⁻¹⁰

NaSO ₃ CF ₃ in diglyme		Binding Energy (eV)					
Sputtering time	0 min	1 min	2 min	3 min	8 min	Peak assignment	Species
C 1s	288.5	289.3	-	-	-	C–O	RCH_2ONa
	284.9	285.5	-	-	-	C–C, C–H	RCH_2ONa
O 1s	535.2	535.8	-	-	-	C–O	RCH_2ONa
	530.7	530.8	530.5	-	-	Na–O	Na_2O
Na 1s	1070.8	1071.3	1071.3	-	-	Na–O, Na–F	$\text{Na}_2\text{O}, \text{NaF}$
F 1s	688.2	-	-	-	-	C–F	CF_3
	683.3	684.0	684.2	-	-	Na–F	NaF
Cu 2p3/2	-	932.5	932.4	932.4	932.4	Cu	Cu

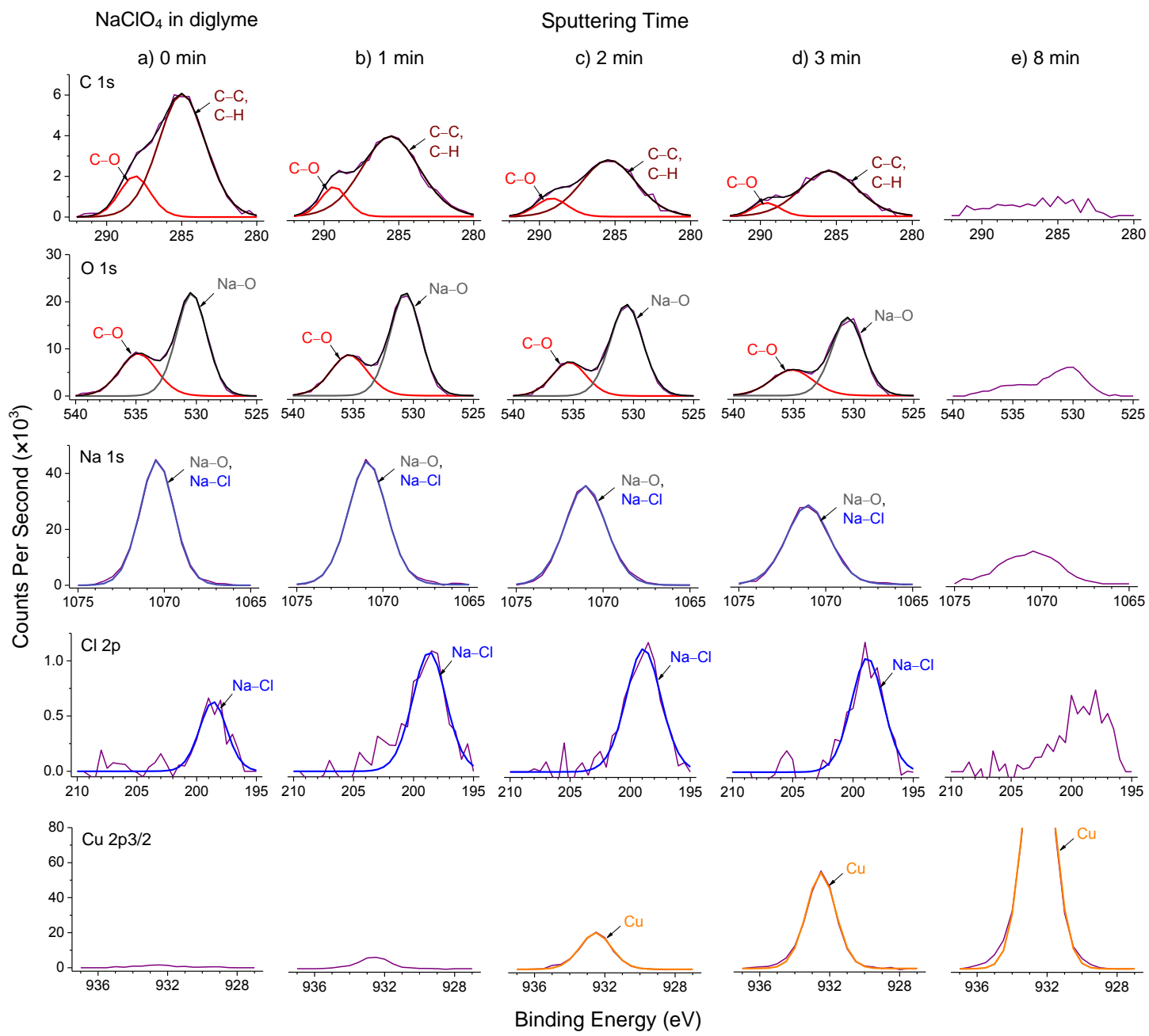


Fig. S20 XPS characterization of the SEI formed using 1 M NaClO₄ in diglyme after **(a)** 0 min, **(b)** 1 min, **(c)** 2 min, **(d)** 3 min and **(e)** 8 min of sputtering. NaClO₄ in diglyme forms a non-uniform and non-compact SEI consisting of organic RCH₂ONa and inorganic Na₂O/NaCl species. NaCl has a lower shear modulus compared to NaF (Table S2), making it less capable of suppressing dendrite growth.

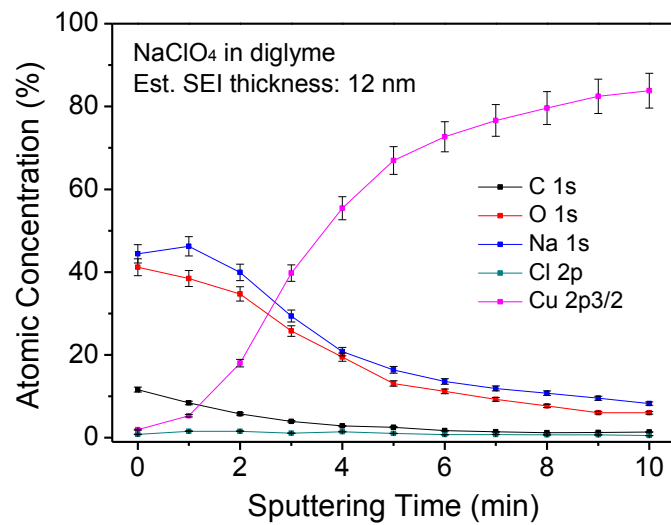


Fig. S21 XPS atomic concentration of various elements as a function of sputtering time for the SEI formed using 1 M NaClO₄ in diglyme.

Table S8 XPS binding energy values and peak assignments of the SEI components formed using 1 M NaClO₄ in diglyme.⁵⁻¹⁰

NaClO ₄ in diglyme		Binding Energy (eV)					
Sputtering time	0 min	1 min	2 min	3 min	8 min	Peak assignment	Species
C 1s	288.1	289.3	289.2	289.6	-	C–O	RCH ₂ ONa
	285.0	285.5	285.4	285.5	-	C–C, C–H	RCH ₂ ONa
O 1s	534.8	535.3	535.3	535.1	-	C–O	RCH ₂ ONa
	530.4	530.7	530.6	530.5	-	Na–O	Na ₂ O
Na 1s	1070.4	1070.9	1071.0	1071.0	-	Na–O, Na–Cl	Na ₂ O, NaCl
Cl 2p	198.6	198.7	198.9	198.8	-	Na–Cl	NaCl
Cu 2p3/2	-	-	932.5	932.5	932.5	Cu	Cu

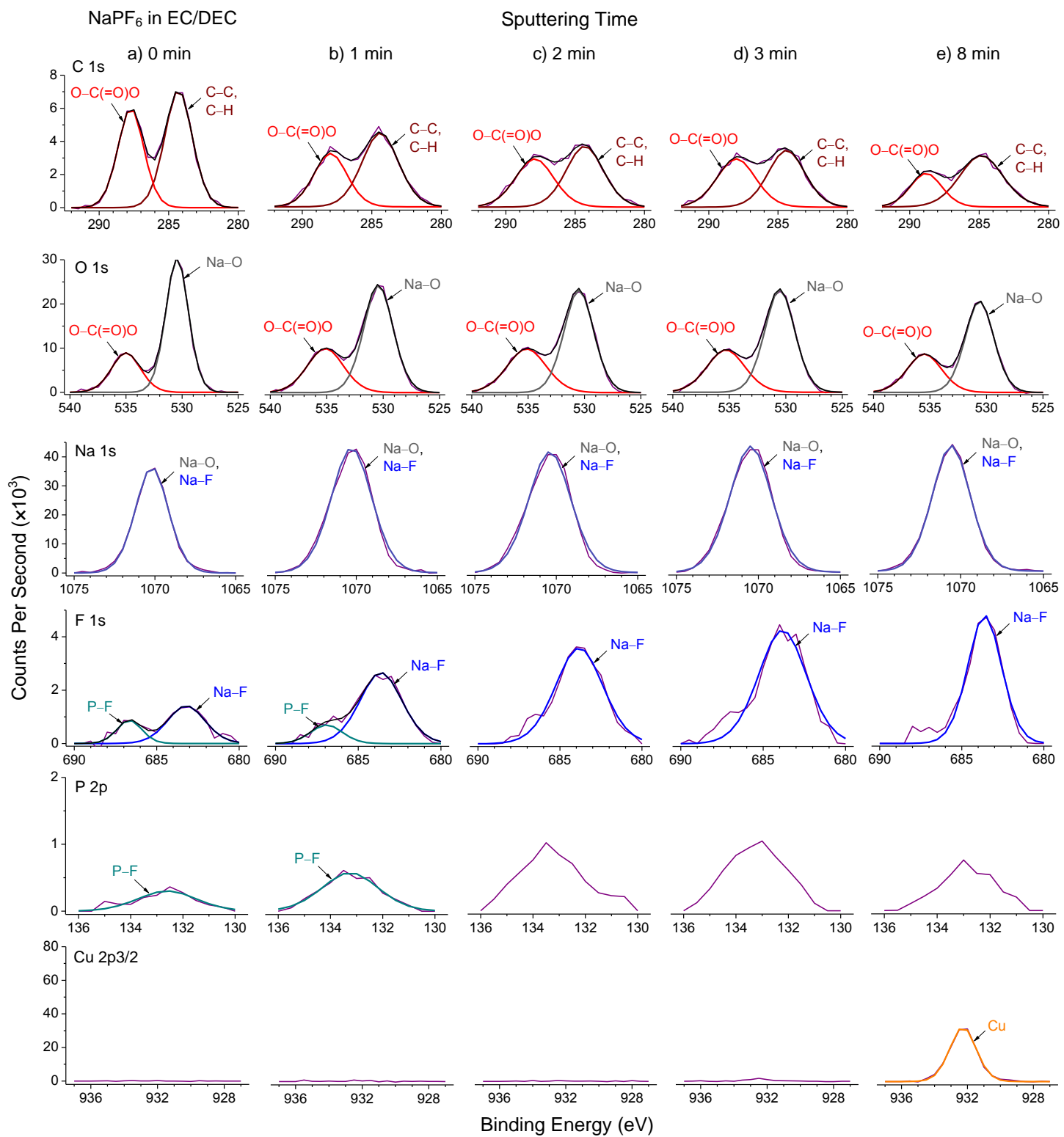


Fig. S22 XPS characterization of the SEI formed using 1 M NaPF₆ in 1: 1 v/v EC/DEC after **(a)** 0 min, **(b)** 1 min, **(c)** 2 min, **(d)** 3 min and **(e)** 8 min of sputtering.

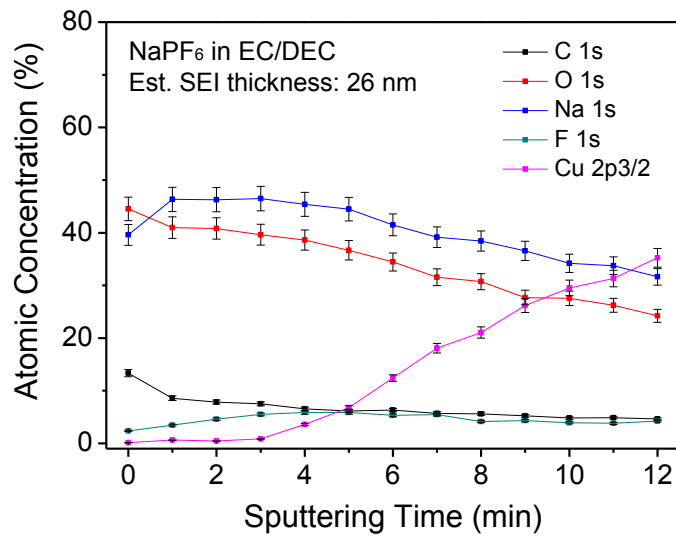


Fig. S23 XPS atomic concentration of various elements as a function of sputtering time for the SEI formed using 1 M NaPF₆ in 1: 1 v/v EC/DEC.

Table S9 XPS binding energy values and peak assignments of the SEI components formed using 1 M NaPF₆ in 1: 1 v/v EC/DEC.⁵⁻¹⁰

NaPF ₆ in EC/DEC		Binding Energy (eV)					Species
Sputtering time	0 min	1 min	2 min	3 min	8 min	Peak assignment	
C 1s	287.7	288.0	287.9	288.0	288.8	O-C(=O)O	(CH ₂ OCO ₂ Na) ₂ , CH ₃ CH ₂ OCO ₂ Na
	284.3	284.4	284.3	284.4	284.8	C-C, C-H	(CH ₂ OCO ₂ Na) ₂ , CH ₃ CH ₂ OCO ₂ Na
O 1s	535.0	535.1	535.1	535.3	535.5	O-C(=O)O	(CH ₂ OCO ₂ Na) ₂ , CH ₃ CH ₂ OCO ₂ Na
	530.4	530.4	530.5	530.5	530.6	Na-O	Na ₂ O
Na 1s	1070.2	1070.2	1070.4	1070.4	1070.6	Na-O, Na-F	Na ₂ O, NaF
F 1s	686.7	686.9	-	-	-	P-F	Na _x PF _y , Na _x PO _y F _z
	683.2	683.6	683.8	683.8	683.6	Na-F	NaF
P 2p	132.6	133.2	-	-	-	P-F	Na _x PF _y , Na _x PO _y F _z
Cu 2p3/2	-	-	-	-	932.3	Cu	Cu

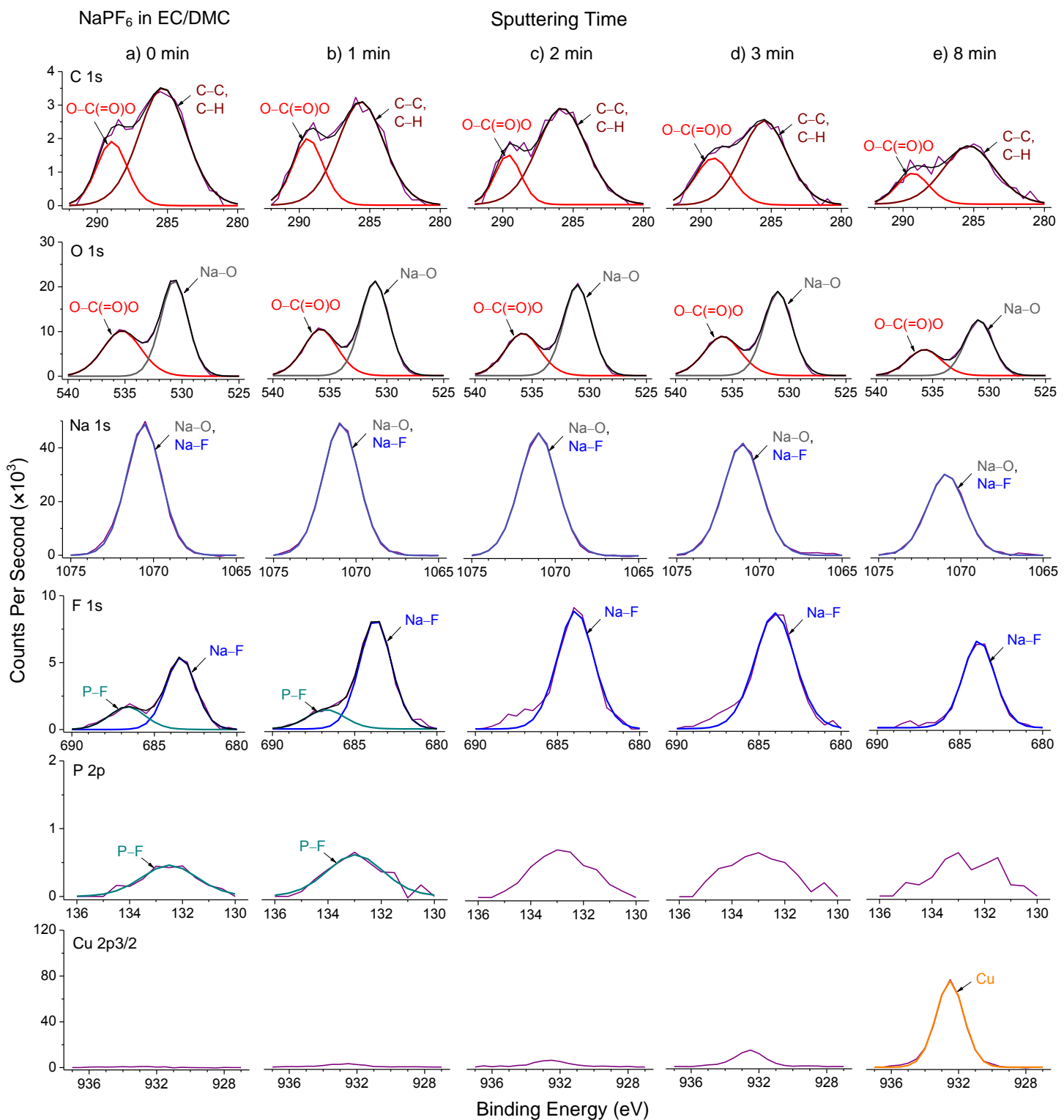


Fig. S24 XPS characterization of the SEI formed using 1 M NaPF₆ in 1: 1 v/v EC/DMC after **(a)** 0 min, **(b)** 1 min, **(c)** 2 min, **(d)** 3 min and **(e)** 8 min of sputtering.

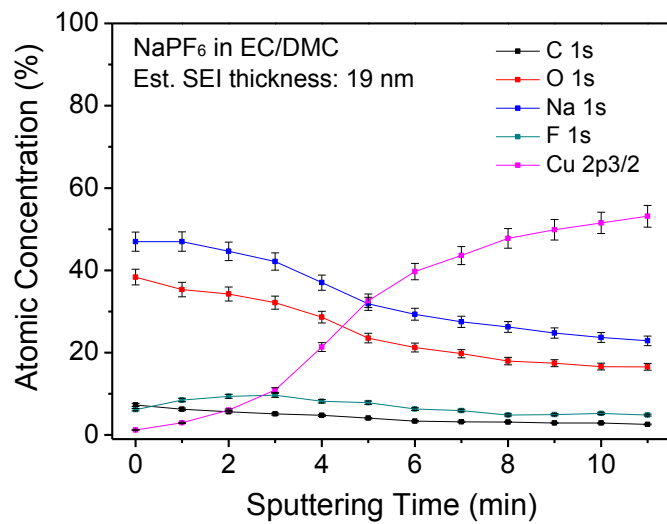


Fig. S25 XPS atomic concentration of various elements as a function of sputtering time for the SEI formed using 1 M NaPF₆ in 1: 1 v/v EC/DMC.

Table S10 XPS binding energy values and peak assignments of the SEI components formed using 1 M NaPF₆ in 1: 1 v/v EC/DMC.⁵⁻¹⁰

NaPF ₆ in EC/DMC		Binding Energy (eV)					Peak assignment	Species
Sputtering time	0 min	1 min	2 min	3 min	8 min			
C 1s	289.0	289.4	289.6	289.1	289.3	O-C(=O)O	(CH ₂ OCO ₂ Na) ₂ , CH ₃ OCO ₂ Na	
	285.3	285.6	285.8	285.5	285.3	C-C, C-H		(CH ₂ OCO ₂ Na) ₂ , CH ₃ OCO ₂ Na
O 1s	535.2	535.8	535.8	535.9	535.7	O-C(=O)O	(CH ₂ OCO ₂ Na) ₂ , CH ₃ OCO ₂ Na	
	530.7	531.0	531.0	531.0	530.9	Na-O		Na ₂ O
Na 1s	1070.6	1070.9	1071.0	1071.0	1070.9	Na-O, Na-F	Na ₂ O, NaF	
F 1s	686.6	686.7	-	-	-	P-F	Na _x PF _y , Na _x PO _y F _z	
	683.4	683.7	683.9	684.0	683.8	Na-F		NaF
P 2p	132.5	133.0	-	-	-	P-F	Na _x PF _y , Na _x PO _y F _z	
Cu 2p3/2	-	-	-	-	932.5	Cu	Cu	

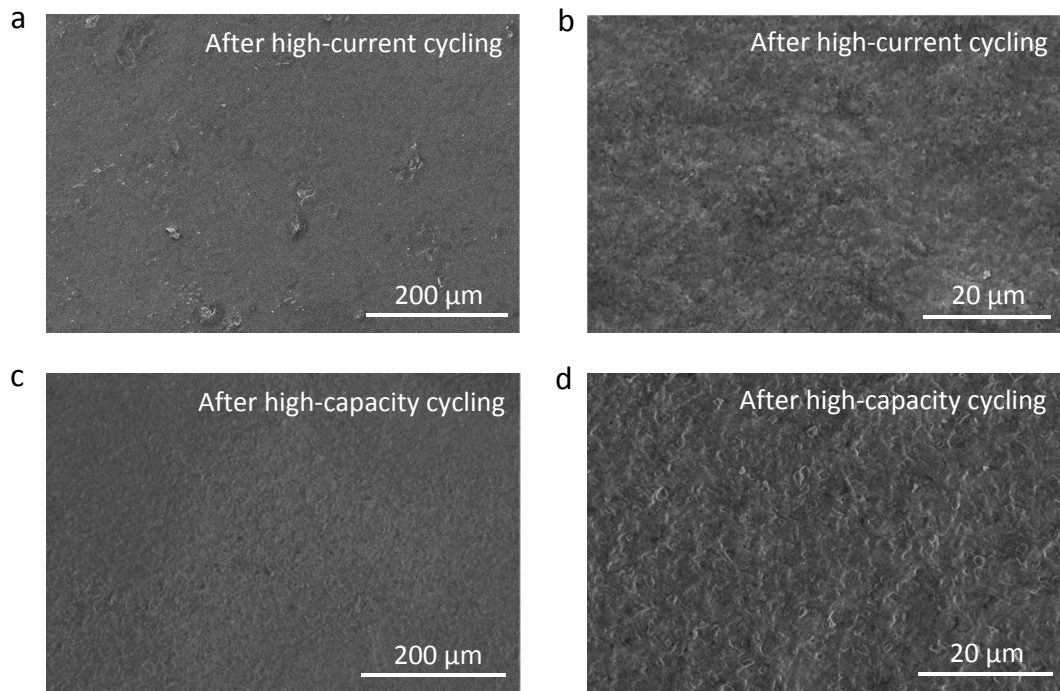


Fig. S26 Low- and high-magnification SEM images of the Na metal surface (**a, b**) after 40 cycles at 1 mAh cm^{-2} with increasing current densities and (**c, d**) after 50 cycles at 1 mA cm^{-2} with increasing areal capacities using 1 M NaPF_6 in diglyme.

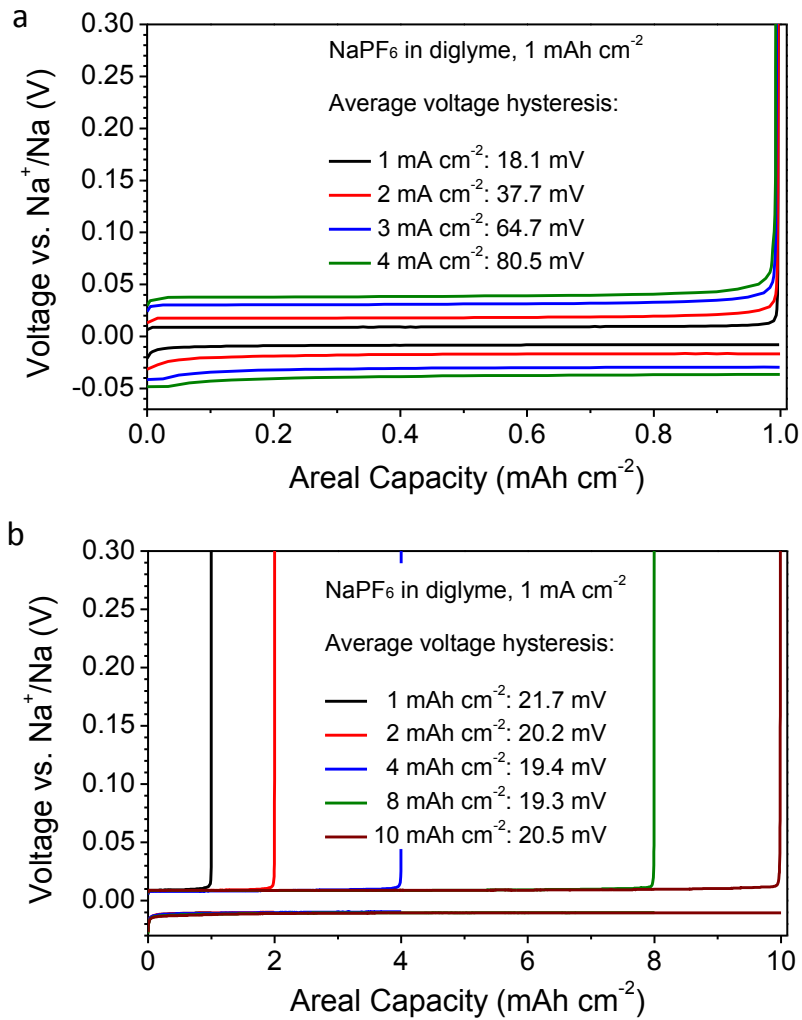


Fig. S27 Plating–stripping voltage profiles and average voltage hysteresis of Na metal anodes cycled at (a) 1 mAh cm^{-2} with increasing current densities and (b) 1 mA cm^{-2} with increasing areal capacities using 1 M NaPF_6 in diglyme.

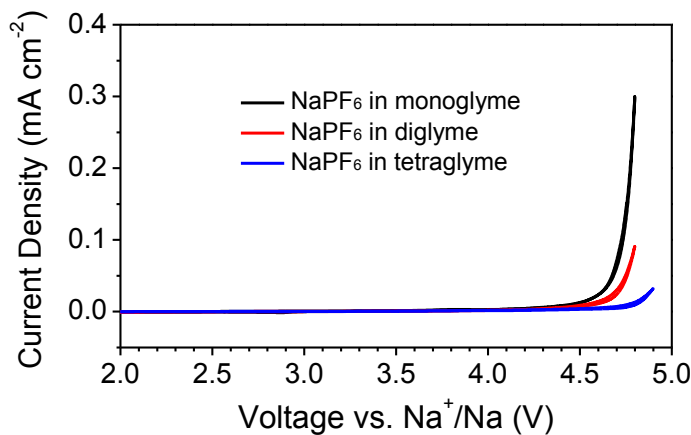


Fig. S28 Cyclic voltammograms showing the onset oxidation potentials of 1 M NaPF_6 in monoglyme, diglyme and tetraglyme (~ 4.4, 4.5 and 4.7 V vs. Na^+/Na respectively). Cyclic voltammetry was carried out using a Bio-Logic VMP3 Potentiostat (scan rate: 0.1 mV s^{-1}) with Pt foil as the working electrode and Na metal as the counter and reference electrodes.

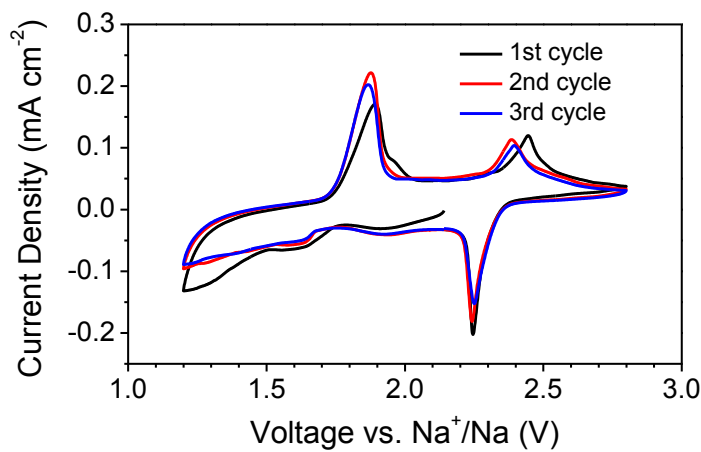


Fig. S29 Cyclic voltammograms of a room-temperature Na–S battery cycled using 1 M NaPF_6 in tetraglyme, carried out using a Bio-Logic VMP3 Potentiostat (scan rate: 0.1 mV s^{-1}) with S/C cathode as the working electrode and Na metal as the counter and reference electrodes.

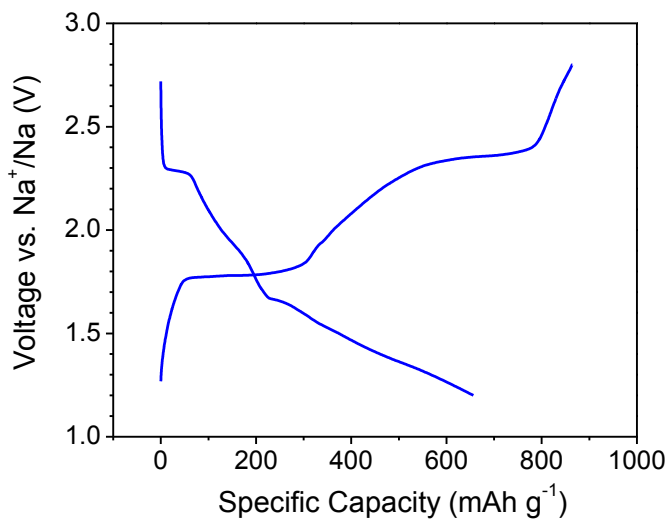


Fig. S30 Typical charge–discharge voltage profile of a room-temperature Na–S battery cycled using 1 M NaPF_6 in tetraglyme. The typical Coulombic efficiency of 74 to 80% is caused by the polysulfide shuttle effect from dissolution of intermediate long-chain polysulfide species into the electrolyte.¹⁶ Further work is ongoing to encapsulate the S cathodes more effectively in suitable host materials to trap the polysulfide species and minimize their dissolution into the electrolyte.

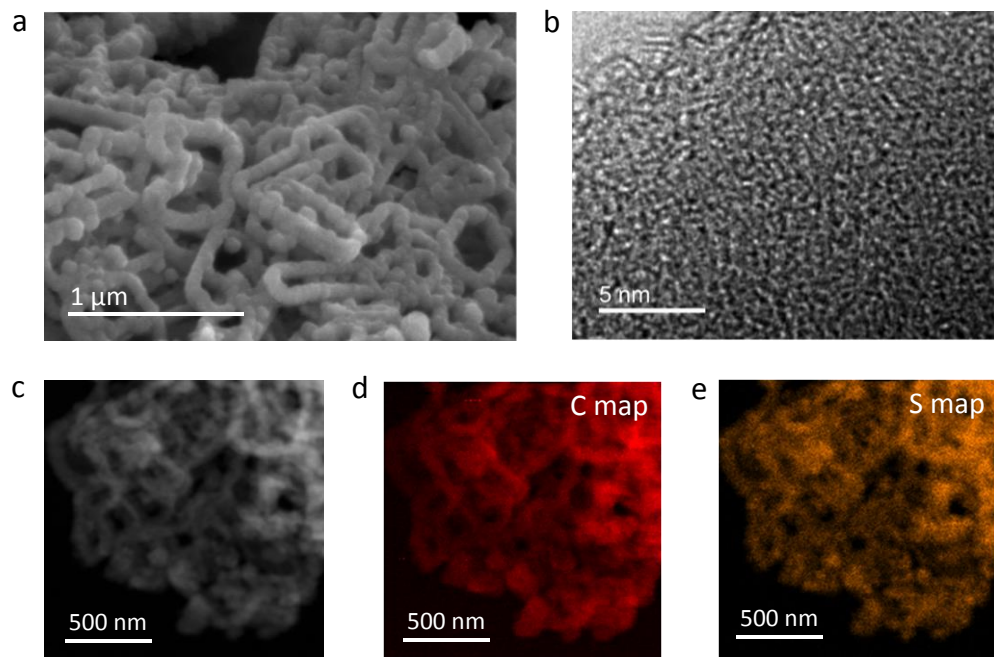


Fig. S31 (a) SEM, (b) High-resolution TEM and (c) STEM images, as well as (d) C and (e) S elemental maps of the S/C composites used as cathodes in room-temperature Na–S batteries.

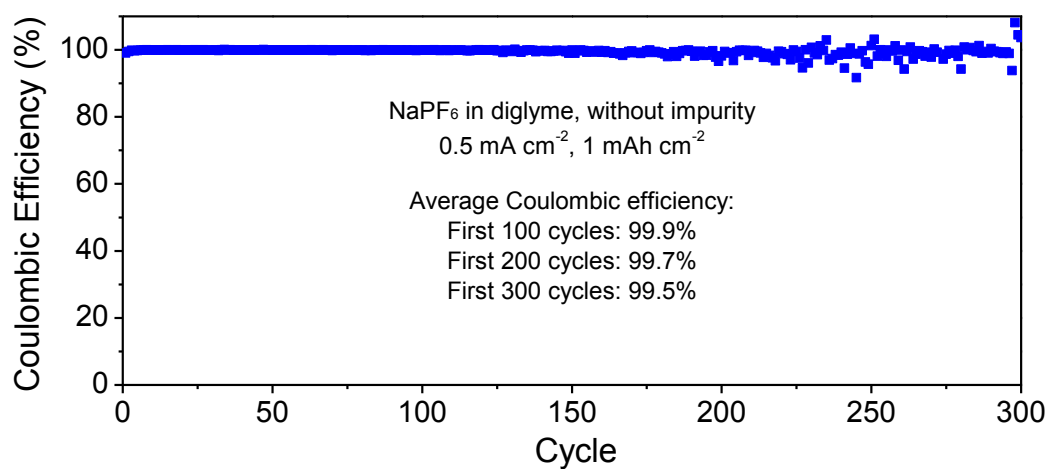


Fig. S32 Plating–stripping Coulombic efficiencies of Na metal anodes cycled using 1 M NaPF_6 in diglyme without impurity, which was obtained by allowing the small amount of insoluble impurity in the as-prepared electrolyte to settle down and extracting the supernatant for use.

References

1. P. G. Bruce, S. A. Freunberger, L. J. Hardwick, J.-M. Tarascon, *Nat. Mater.* **11**, 19-29 (2012).
2. K. B. Hueso, M. Armand, T. Rojo, *Energy Environ. Sci.* **6**, 734-749 (2013).
3. S. Wenzel *et al.*, *J. Power Sources* **243**, 758-765 (2013).
4. P. Hartmann *et al.*, *Nat. Mater.* **12**, 228-232 (2013).
5. K. Xu, *Chem. Rev.* **104**, 4303-4417 (2004).
6. K. Xu, *Chem. Rev.* **114**, 11503-11618 (2014).
7. P. Verma, P. Maire, P. Novak, *Electrochim. Acta* **55**, 6332-6341 (2010).
8. D. Aurbach *et al.*, *J. Electrochem. Soc.* **156**, A694-A702 (2009).
9. A. Budi *et al.*, *J. Phys. Chem. C* **116**, 19789-19797 (2012).
10. J. F. Moulder, J. Chastain, *Handbook of X-ray photoelectron spectroscopy: a reference book of standard spectra for identification and interpretation of XPS data*. Physical Electronics Division, Perkin-Elmer Corp., 1995.
11. G. W. C. Kaye, T. H. Laby, *Tables of physical and chemical constants*, Longman, London, UK, 15th edition, 1993.
12. A. M. James, M. P. Lord, *Macmillan's chemical and physical data*, Macmillan, London, UK, 1992.
13. G. V. Samsonov (Ed.), *Handbook of the physicochemical properties of the elements*, IFI-Plenum, New York, USA, 1968.
14. Y. N. Zhuravlev, O. S. Obolonskaya, *Russ. Phys. J.* **53**, 776-784 (2011).
15. R. S. Carmichael (Ed.), *Handbook of physical properties of rocks*, CRC Press, 1982.
16. A. Manthiram, X. Yu, *Small* **11**, 2108-2114 (2015).